

Uncovering and tailoring hidden Rashba spin-orbit splitting in centrosymmetric crystals

Linding Yuan^{1,2}, Qihang Liu^{3,4}, Xiuwen Zhang⁵, Jun-Wei Luo^{1,2,6*}, Shu-Shen Li^{1,2,6}, and Alex Zunger^{4*}

¹*State Key Laboratory for Superlattices and Microstructures, Institute of Semiconductors, Chinese Academy of Sciences, PO Box 912, Beijing 100083, China*

²*College of Materials Science and Opto-Electronic Technology, University of Chinese Academy of Sciences, Beijing, China*

³*Department of Physics, Southern University of Science and Technology, Shenzhen 518055, China*

⁴*Renewable and Sustainable Energy Institute, University of Colorado, Boulder, CO 80309, USA*

⁵*College of Electronic Science and Technology, Shenzhen University, Guangzhou, China*

⁶*Beijing Academy of Quantum Information Sciences, Beijing 100193, China*

*Email: jwluo@semi.ac.cn; alex.zunger@colorado.edu

Hidden Rashba and Dresselhaus spin-splittings in centrosymmetric crystals with subunits (sectors) having non-centrosymmetric symmetries (the R-2 and D-2 effects) have been predicted and observed experimentally, but the microscopic mechanism remains unclear. Here we demonstrate that the spin-splitting in R-2 is enforced by specific symmetries (such as the non-symmorphic in the present example) which ensures that the pertinent spin wavefunctions segregate spatially on just one of the two inversion-partner sectors and thus avoid compensation. This finding establishes a common fundamental source for the conventional Rashba (R-1) effect and the R-2 effect, both originating from the *local* sector symmetries, rather than from the *global* crystal asymmetry alone for R-1 per se. We further show that the effective Hamiltonian for the R-1 effect is also applicable for the R-2 effect, but applying a symmetry-breaking electric field to an R-2 compound produces different spin-splitting pattern than applying a field to a trivial (non-R-2) centrosymmetric compound.

Numerous physical effects and the technologies enabled by them are conditional on the presence of certain symmetries in the material that hosts such effects. Examples include effects predicated on the *absence of inversion symmetry* (non-centrosymmetric systems) such as the Dresselhaus effect¹; the Rashba effect²; optical activity in non-chiral molecules³; valley polarization and its derivative effects⁴; and valley Hall effect in 2D layered structures⁵. While centrosymmetric systems are supposed to lack those effects, there is a large class of systems whose global crystal symmetry (GCS) is indeed centrosymmetric, but they consist of individual sectors with non-centrosymmetric local sector symmetry (LSS) (non-centrosymmetric site point groups). “Hidden effect” refers to the general conditions where the said effect does exist even when the nominal GCS would disallow it. For example, the hidden Dresselhaus effect⁶ occurs in the diamond-type structure of Silicon, where each atom has a non-centrosymmetric LSS (the tetrahedral T_d point group), but the crystal as a whole has a centrosymmetric GCS (the octahedral O_h group). The theoretical prediction⁶ and subsequent experimental observations⁷⁻¹² of “hidden spin polarization” in nonmagnetic centrosymmetric crystals triggered research on broader physical effects nominally disallowed under high GCS of systems, such as optical activity¹³, intrinsic circular polarization¹⁴, current-induced spin polarization^{15,16}, superconductor¹⁷, piezoelectric polarization⁶, and orbital polarization¹⁸ in various centrosymmetric systems, as summarized in Table I.

We use the designation “1” for cases where global inversion symmetry is absent, (and, thus, exhibiting the physical effects conditional on the absence of global inversion symmetry), as is the case of the conventional Rashba effect (R-1) or Dresselhaus effect (D-1). In parallel, we use the designation “2” for cases where the presence of global inversion symmetry hides the physical effects (conditional on the absence of symmetry), which is but revealed theoretically⁶ and observed experimentally⁷⁻¹². The latter is the case for the hidden Rashba effect (R-2) or hidden Dresselhaus effect (D-2)⁶. Note that in R-2 or D-2 nonmagnetic materials, even though the local spin polarization is nonzero, the net spin polarization remains zero (spin degeneracy), as imposed by the global inversion symmetry.

In our previous work Ref. 6, the idea of hidden spin polarization and the general conditions for its existence -- global inversion symmetry and existence of inversion-partner sectors with non-centrosymmetric site point group symmetries-- was introduced. In the

present work, we focus on the microscopic mechanisms at play and how can they be translated into “design principles “for selecting high-quality R-2 materials for future experiments. We (i) show a common denominator for both R-1 and R-2 Rashba splitting, i.e. both effects originate from the symmetries of the local inversion-partner sectors rather than the global symmetries of the systems. (ii) Since net spin polarization requires that the doubly degenerate states on the different sectors be prevented from mixing, we point out the mechanism of symmetry-enforced wavefunction segregation, that prevents the doubly degenerate states on the different sectors from otherwise mixing. This is illustrated for the prototype compound in BaNiS₂ where the requisite symmetry is the non-symmorphic operation. (iii) To clarify the difference between an R-2 compound and a trivial centrosymmetric compound we investigate the evolution of the R-1 spin-splitting from a symmetry-broken R-2 spin-splitting (“R-1-from-R-2”) by placing a tiny electric field on R-2 that breaks the global inversion symmetry. We find that even for a tiny applied field the ensuing α_R of “R-1-from-R-2” far exceeds the effect “R-1 from trivial centrosymmetric” compound, highlighting the facts that the observed R-2 spin-splitting is not due to inadvertent breaking of the inversion symmetry in an ordinary centrosymmetric compound as recently thought¹⁹. This shows that ARPES experiments can indeed probe band splitting genuinely coming from the hidden spin-splitting, even if they are affected by surface sensitivity. This solves another criticism raised by Ref. 19 against the hidden spin polarization detection, namely the attribution of spin-splitting to surface effects rather than to the bulk. This work sheds light on the view of the recent debate around the physical meaning and relevance of the "hidden spin polarization" concept, and for the strong experimental and theoretical activity around it, motivated by the possibility to device materials with remarkable spin textures and technologically relevant properties. This work also offers clear experimental and computational frameworks to understand, tailor and utilize the R-2/D-2 effects.

The evolution of R-2 into R-1 under an inversion-symmetry-breaking electric field

One might naively think that the observed R-2 spin-splitting is due to inadvertent breaking of the inversion symmetry in an ordinary centrosymmetric compound.²¹ Indeed, a centrosymmetric R-2 compound is distinct from a trivial centrosymmetric compound in

that the former consist of individual polar sectors with non-centrosymmetric LSS (specifically, polar site point groups C_1 , C_2 , C_3 , C_4 , C_6 , C_{1v} , C_{2v} , C_{3v} , C_{4v} and C_{6v}). A tiny electric field applied to a *centrosymmetric trivial* material such as cubic perovskites²⁰ gives rise to a proportionally tiny spin-splitting whose magnitude is proportional to the field. To clarify the difference between an R-2 compound and a trivial centrosymmetric compound often confused¹⁹, we investigate the evolution of the R-1 spin-splitting from a symmetry-broken R-2 spin-splitting (“R-1-from-R-2”) by using the first-principles calculations on R-2 compounds and placing on it a tiny electric field that breaks the global inversion symmetry, but conserves the time reversal symmetry.

An example of R-2 compounds is BaNiS_2 ¹⁰, which is a five-coordinated Ni(II) structure consisting of puckered two-dimensional layers of edge-sharing square pyramidal polyhedral and crystalizes in the tetragonal system, space group $P4/nmm$. Conductivity and susceptibility measurements^{21,22} indicate that it is a metallic Pauli Paramagnet. Our DFT+U calculation ($U=3\text{eV}$, $J=0.95\text{eV}$) also predicts a low-temperature anti-ferromagnetic phase with local Ni moments of $\pm 0.7 \mu\text{B}$ for bulk ($\pm 0.6 \mu\text{B}$ for a monolayer) where the anti-ferromagnetic phase is slightly more stable than the non-magnetic model by just 43 meV/f.u for bulk and 28 meV/f.u for monolayer. These DFT+U calculations had reported that BaNiS_2 undergoes a phase transition from paramagnetic to antiferromagnetic as increasing the used U value from 2 to 3 eV. Given the difficulty of estimating the proper U value in the +U framework and experimental (conductivity and susceptibility) observation^{21,22} of metallic Pauli Paramagnet, in this work, we nevertheless adopt a non-magnetic phase for BaNiS_2 to avoid the unnecessary complications from magnetic orders. Our relaxed lattice constants and interatomic distances in the non-magnetic GGA calculation agrees with the measured result within $\sim 1\%$ s^{10,21}. In the non-magnetic model BaNiS_2 possesses both inversion symmetry and time-reversal symmetry; in the presence of SOC, each energy band is even-fold degenerate and thus has no R-1 spin-splitting.

Figure 1a shows the structure of a monolayer of this centrosymmetric crystal, which has two separated crystallographic sectors -- S_α and its inversion-partner S_β (shown in Figure 1a as red and blue planes, respectively); each sector contains a single B atom (here, $B = \text{Ni, Pd, or Pt}$) with a polar site group C_{4v} , having its local internal dipole field¹⁰ (calculated and shown below). We focus our attention on the lowest four conduction bands

(including spin) around the \bar{X} point (highlighted with a red square in Figure 1b). Figure 1c shows that when SOC is turned off in the first-principles calculations, one finds along high-symmetry path $\bar{X} - \bar{M}$ a single, four-fold degenerate band whose degeneracy is imposed by the non-symmorphic screw-axis symmetry $\{C_{2x}|(a/2, 0, 0)\} ; \{C_{2y}|(0, a/2, 0)\}$ (explained in supplementary section B). When SOC is turned on, the four-fold degenerate band splits into two branches A and B (Figure 1d), and each branch is doubly degenerate and has two orthogonal spin components.

The spin-degeneracy of both branches A and B along $\bar{X} - \bar{M}$ as well as at the \bar{X} point is lifted upon application of an external electric field E_{ext} , as shown in Figure 1e. This splitting denoted $\Delta_{\alpha\beta}$ occurs at the time-reversal invariant (TRI) \bar{X} point and is dependent linearly on E_{ext} (see Figure 3b). The finite splitting at the TRI point rules out the Rashba effect as the origin of the splitting of the two spin components of branch A (and branch B) along $\bar{X} - \bar{M}$. Figure 2a indeed shows that the spin-down component of the high-energy branch A and the spin-up component of the low-energy branch B have wavefunctions confined in sector S_α , and thus pair as one orbital band (hereafter, termed S_α -Rashba-band). The spin-up component of the branch A and the spin-down component of the branch B possess wavefunctions confined in sector S_β (hereafter, termed S_β -Rashba-band). We therefore identify the splitting $\delta E_{AB}(k)$ as a consequence of the R-2 effect quantified by a Rashba parameter α_R (R-2) = 0.24 VÅ. The applied electric field further adds/subtracts the R-1 spin-splitting to/from the R-2 splitting $\delta E_{AB}(k)$ of the S_α - and S_β -Rashba-band, respectively, along $\bar{X} - \bar{M}$ direction. Figure 3a shows the corresponding Rashba parameters $\alpha_R = \delta E_{AB}(k - \bar{X})/2(k - \bar{X})$, which exhibits a linear response to E_{ext} : α_R of the S_α -Rashba-band increases, and the S_β -Rashba-band decreases at rates of the same magnitude but opposite sign as increasing E_{ext} . The extrapolations of these two α_R functions cross at $E_{ext} = 0$, giving rise to $\alpha_R = 0.24$ VÅ, a value being the same as the (zero-field) R-2 spin splitting α_R (R-2).

The magnitude of the R-2 spin-splitting can be determined unambiguously by placing on a candidate R-2 compound an electric field, then extrapolating to the zero field to uncover a finite, zero-field (R-2) Rashba parameter. *The significant magnitude illustrated above of the ensuing α_R of “R-1-from-R-2” relative to “R-1 from trivial centrosymmetric”*

compound highlights the fact that the R-1 spin-splitting is inherited from the R-2 effect in bulk Rashba systems, i.e., from the local asymmetric dipole fields of the individual sectors. This finding obviates the concern of Li and Appelbaum¹⁹ who suggested that the Rashba surface spin-splitting detected experimentally (e.g., via ARPES) might originate from the unavoidable inversion-symmetry-broken surface since this contribution is indistinguishable from bulk R-2 effect.

Avoided compensation of the R-2 spin polarization in BaNiS₂ by non-symmorphic symmetry

We next clarify under what circumstances the hidden R-2 effect can be large or small. This physics can be gleaned by looking at a single nonmagnetic centrosymmetric R-2 ABX₂ system in two different directions in the Brillouin zone. Figure 1 shows that these R-2 bands along $\bar{X} - \bar{M}$ and $\bar{X} - \bar{\Gamma}$ directions exhibit two different types of spin-splitting behaviors associated with the distinct transformation properties of the wavefunction under *non-symmorphic glide reflection symmetry* (see supplementary section B for details). This realization then would help us establish the distinguishing features of R-1 vs. R-2 materials.

(a) Wavefunction segregation causes sizable R-2 spin-splitting along $\bar{X} - \bar{M}$ direction

To quantify the degree of wavefunction segregation (DWS), we introduce a measure $D(\varphi_{\mathbf{k}})$ for states $\varphi_{\mathbf{k}}$ at the wavevector \mathbf{k} , where

$$D(\varphi_{\mathbf{k}}) = \left| \frac{P_{\varphi_{\mathbf{k}}}(S_{\alpha}) - P_{\varphi_{\mathbf{k}}}(S_{\beta})}{P_{\varphi_{\mathbf{k}}}(S_{\alpha}) + P_{\varphi_{\mathbf{k}}}(S_{\beta})} \right|, \quad (1)$$

and

$$P_{\varphi_{\mathbf{k}}}(S_{\alpha,\beta}) = \int_{\Omega \in S_{\alpha,\beta}} |\varphi_{\mathbf{k}}(\mathbf{r})|^2 d^3\mathbf{r}. \quad (2)$$

$P_{\varphi_{\mathbf{k}}}(S_{\alpha})$ is the component of the wavefunction $\varphi_{\mathbf{k}}$ localized on the sector S_{α} . The DWS explicitly quantifies the locality of wavefunction, in contrast to, the implicit measure¹⁰ by means of the integral of the local spin density operator restricted on a given sector.

It is evident that $D(\varphi_{\mathbf{k}}) = 0$ for a wholly delocalized wavefunction over two inversion-partner sectors, whereas, $D(\varphi_{\mathbf{k}}) = 100\%$ indicates that the wavefunction is entirely confined either on sector S_{α} or sector S_{β} . One expects, in general, that any linear combination of two degenerate states should still be an eigenstate and prevents us from

obtaining a unique DWS for the energy degenerate bands.¹⁹ However, we demonstrated in supplementary section B that, in R-2 compounds, the symmetry of the wavevectors along $\bar{X} - \bar{M}$ direction prohibits the mixing of two degenerate states arising from two inversion-partner sectors (S_α and S_β), respectively, as a result of the *glide reflection* symmetry, and hence dissociates any linear combinations of the degenerate states for tracing back to the symmetry enforced segregated states. Santos-Cottin, et al.¹⁰ had shown the localization of wavefunction in BaNiS₂ to provide the basis to decouple two effective Rashba Hamiltonians associated with each sector. Our calculations also (Fig. 2a) show segregated wavefunctions (localized either on sector S_α or S_β) and $D(\varphi_{\mathbf{k}}) = 88\%$ ($\mathbf{k} = (0.025, 0.5, 0)(2\pi/a)$, here a is the lattice constant, for both spin components of doubly degenerate branches A and B along $\bar{X} - \bar{M}$ direction. This fact obviates the concern of validity of hidden spin-splitting theory due to the possible lack of gauge invariance, raised by Li and Appelbaum¹⁹.

The relation between wavefunction segregation and the R-2 effect can be appreciated as follows: In two-dimensional quantum wells or heterojunctions, one obtains the Rashba parameter α_R due to the R-1 effect as²³

$$\alpha_{R,i} = \langle r_{R,i} \cdot \mathbf{E}(\mathbf{r}) \rangle \quad (3)$$

where $r_{R,i}$ is a material-specific Rashba coefficient of the i th-band, the electric field $\mathbf{E}(\mathbf{r}) = (1/e)\nabla V$ is the local gradient of the crystal potential V , and angular brackets indicate an average of the local Rashba parameter $r_{R,i}\mathbf{E}(\mathbf{r})$ of the well and barrier materials weighted by the wavefunction amplitude. In a crystal without external fields, the electric field originates from the local dipole and is termed $\mathbf{E}_{dp}(\mathbf{r})$, which does not have to vanish at all atomic sites even in centrosymmetric systems. Figure 2e shows the z-component of the internal local dipole fields $E_{dp}(z)$ in the monolayer BaNiS₂. It exhibits that $E_{dp}(z)$ varies rapidly within a single sector and is inversion through a point located on the Sulphur atom (or point reflection). The internal dipole fields are finite (and in fact atomically large) within a single sector, whereas the sum over both inversion-partner sectors is zero as expected. The *segregation of wavefunctions on a single sector* with $D(\varphi_{\mathbf{k}}) = 88\%$ for states along $\bar{X} - \bar{M}$ direction indicates that this band experiences a net effective field of the internal dipole fields within a single sector (as illustrated in Figure 2f), and is immune to

full compensation from the opposite dipole fields within its inversion-partner sector. According to Equation (3), a finite Rashba parameter α_R is thus obtained for R-2 bands along $\bar{X} - \bar{M}$ direction. *Thus, the large R2 effect along this BZ direction originates from wavefunction segregation on each of the two inversion-partner sectors, avoiding mutual compensation of local dipolar electric fields.*

(b) Wavefunction delocalization leads to vanishing R-2 spin-splitting along the $\bar{X} - \bar{\Gamma}$ direction

In sharp contrast to the $\bar{X} - \bar{M}$ direction, Figure 1c shows that along $\bar{X} - \bar{\Gamma}$ direction these four bands already split into two doublets even in the absence of SOC, and the magnitude of their splitting is barely changed after turning on the SOC. We attribute such band splitting to symmetry allowed interaction between states stemming from two inversion-partner sectors S_α and S_β (see supplementary section B). Thereby, we denote two spin components of the branch A by $S_{\alpha/\beta}^\downarrow(A, k_{\bar{X}-\bar{\Gamma}})$ and $S_{\alpha/\beta}^\uparrow(A, k_{\bar{X}-\bar{\Gamma}})$, respectively, whereas, for branch B we use $S_{\alpha/\beta}^\downarrow(B, k_{\bar{X}-\bar{\Gamma}})$ and $S_{\alpha/\beta}^\uparrow(B, k_{\bar{X}-\bar{\Gamma}})$. The wavefunction of the spin down component of the branch A is 49% confined and that of branch B is 51% confined in sector S_α , respectively, so as Figure 2b shows DWS is $D(S_{\alpha/\beta}^\downarrow(A, k_{\bar{X}-\bar{\Gamma}})) = D(S_{\alpha/\beta}^\downarrow(B, k_{\bar{X}-\bar{\Gamma}})) = 2\%$ for spin down components of both A and B branches. Similarly, the wavefunction of the spin up component of the branch A is 43% confined, and that of branch B is 57% confined in sector S_α so DWS $D(S_{\alpha/\beta}^\uparrow(A, k_{\bar{X}-\bar{\Gamma}})) = D(S_{\alpha/\beta}^\uparrow(B, k_{\bar{X}-\bar{\Gamma}}))$ is 14% for spin up components. Thus, the wavefunctions of the $\bar{X} - \bar{\Gamma}$ bands are essentially delocalized over both inversion-partner sectors S_α and S_β . Such wavefunction delocalization naturally leads to a complete compensation of the undergoing local internal dipole fields within S_α by that within S_β , when each local dipole weighted by its wavefunction amplitudes gives rise to zero average Rashba parameter α_R according to Eq. (3).

Unification of R-1 and R-2 into a single theoretical framework

The smooth “R-1-from-R-2” evolution (Fig. 3a) suggests that when applying an external electric field \mathbf{E}_{ext} to an R-2 system, the electric field $\mathbf{E}(\mathbf{r})$ acting on electrons is a superposition of \mathbf{E}_{ext} and the internal local dipole (dp) electric fields $\mathbf{E}_{dp}(\mathbf{r})$,

$$\mathbf{E}(\mathbf{r}) = \mathbf{E}_{dp}(\mathbf{r}) + \mathbf{E}_{ext}. \quad (4)$$

Thus, both R-1 and R-2 spin-splitting have a common fundamental source, being the dipole electric fields of the local sectors, rather than from the global crystal asymmetry alone for R-1 per se. Such local dipole electric field ‘lives’ within individual local sectors. The fundamental difference between R-1 and R-2 effects is that in R-2 the spin-splitting is hidden by the overlapping energy bands arising from two inversion-partner sectors, whereas in the R-1 case such overlap is forbidden by the global inversion asymmetry.

Figure 1e also shows that the applied electric field lifts the spin degeneracy of the bands along $\bar{X} - \bar{\Gamma}$ direction and raises α_R linearly from zero at $E_{ext} = 0$ to saturation at $E_{ext} = 10 \text{ mV}/\text{\AA}$ at an odd large rate. This behavior is in striking contrast to the linear field-dependence of the bands along $\bar{X} - \bar{M}$ direction (see Figure 3a). Such unusual field-dependence of α_R confirms again that the R-2 spin-splitting evolves smoothly to the R-1 spin-splitting upon the breaking of the global inversion symmetry, regarding the bands along $\bar{X} - \bar{\Gamma}$ direction have vanishing R-2 spin-splitting with $\alpha_R(R2) = 0$ in the absence of an external field. Upon application of electric field, the delocalized wavefunctions of the $\bar{X} - \bar{\Gamma}$ bands become gradually segregated on one of two inversion-partner sectors as a result of Stark effect²⁴. Subsequently, Figure 3c shows that the applied field amplifies the DWS (Eq. (1)) of the spin up component of both branches from 14% to >80% as E_{ext} increases from 0 to $50 \text{ mV}/\text{\AA}$. However, $D(\varphi_{\mathbf{k}})$ is barely changed once $E_{ext} > 50 \text{ mV}/\text{\AA}$ (saturation field). Note that DWS of the corresponding spin down components is not shown but has a similar response to the applied electric field. It is straightforward to learn that the internal electric dipole fields acting on these bands become uncompensated as their wavefunctions change into segregation on a single sector, evoking the R-2 effect with its strength highly related to $D(\varphi_{\mathbf{k}})$ according to Equation (3). The rapid amplification of $D(\varphi_{\mathbf{k}})$ by the applied electric field explains that the (unusual) rapid rise of α_R for those bands along $\bar{X} - \bar{\Gamma}$ direction is mainly due to the enhancement of the wavefunction segregation rather than to the increase of the total electric dipole field.

When E_{ext} reaches ~ 25 mV/Å, α_R of both high and low energy doublets become linear field-dependent but in rates of opposite signs, which is in a similar field-dependence as that along $\bar{X} - \bar{M}$ direction. Figure 3c shows that the response of $D(\varphi_k)$ of the $\bar{X} - \bar{M}$ bands to E_{ext} is, however, barely modified by the external field, indicating those states remain fully localized on one of two inversion-partner sectors. The linear change of α_R along $\bar{X} - \bar{M}$ direction as shown in Figure 3a thus arises entirely from the external field induced asymmetry, i.e., in Equation (3) the change α_R is solely arising from the electric field. The calculated Rashba parameter of the R-2 spin-splitting can be explained regarding the model of the R-1 spin-splitting (Eq. (3)), indicating a unified theoretical view for both R-1 and R-2 effects in bulk systems. *Specifically, the effective electric field that promotes either R-1 and/or R-2 Rashba effects is a superposition of the applied external electric field plus the internal local electric fields originating from the dipoles of the individual local sectors, weighted by the wavefunction amplitude on the corresponding sectors.*

Design principle for increasing the strength of the R-2 effect: R-2 materials⁶ are defined by having global inversion symmetry and two recognizable inversion-partner sectors with polar site point group symmetries (whereas layered structures make the identification of sectors easy, this applies also to non-layered materials as illustrated in Supplementary S1 for rhombohedral SnTe). Designing R-2 materials possessing large hidden spin-splitting and hence strong local spin polarization can benefit from two additional design principles:

(i) Minimizing the mixing and entanglement of the doubly degenerated wavefunctions arising from the two inversion partners sectors. Here, we point to a nontrivial mechanism of symmetry-enforced wavefunction segregation, preventing the doubly degenerate states arising from the different sectors from mixing (in contrast to the trivial physical separation of the two inversion-partner sectors). Note that R-1 compounds do not have to maintain segregation-inducing symmetries to have Rashba effect because its inversion asymmetry alone ensures the avoidance of wavefunction entanglement by lifting the degeneracy of states from the two partner sectors. The wavefunction segregation enforcing symmetry illustrated here is the non-symmorphic symmetry for bands along the $\bar{X} - \bar{M}$ direction in the BaNiS₂ BZ. Other segregation enforcing symmetry operations may exist in general cases, but they have not been discovered yet.

(ii) Instilling strong local dipole fields i.e. designing individual sectors with maximal asymmetry of the local potential within the sector. Thus, whereas the creation and enhancing Rashba effect in conventional (e.g., interfacial) Rashba materials^{2,23} entails, by tradition, breaking inversion symmetry, here our design principles for Rashba effect in centrosymmetric compounds focuses on using other symmetry operations that enhance segregation and avoid mixing. Applying the design principles (i) and (ii) one could design strong R-2 materials via selecting compounds where the wavefunctions are concentrated in real space locations that have a larger magnitude of local dipole fields. An example illustrated here is BaNiS₂. Such wavefunction segregation can be tailored through applying external electric field, strain, atom mutation, or modifications of the polar cation ordering.²³ This is illustrated by the rapid rise of α_R vs. field for bands along $\bar{X} - \bar{\Gamma}$ direction (Fig. 3a) illustrating tailoring R-2 effect. For instance, Otani and his co-workers²⁵ have recently found a strong correlation between the charge density distribution and the strength of the Rashba effect at non-magnetic metal/Bi₂O₃ interfaces. Furthermore, the unexpected rapid rise of α_R vs. field for bands along $\bar{X} - \bar{\Gamma}$ direction (Fig. 3a) implies that one might effectively tune the strength of R-2 effect. We thus present an alternative mechanism for boosting the strength of the Rashba effect, which is commonly achieved by enhancing the breaking of inversion symmetry.

Acknowledgments

J.W.L was supported by the Key Research Program of the Chinese Academy of Sciences (Grant No. XDPB08), the strategic priority research program of the Chinese Academy of Sciences, grant No. XDPB0602, and the National Young 1000 Talents Plan. Work of A.Z. and Q.L at CU Boulder was supported by Department of Energy, Office of Science, Basic Energy Science, MSE division under grant DE-FG02-13ER46959 to CU Boulder.

Author contributions

L.Y. performed the electronic structure calculations, prepared the figures, and developed the tight-binding models with the help of Q.L. J.L. proposed the research project. J.L. and A.Z. established the project direction and conducted the analysis, discussion and writing of the paper with input from L.Y., Q.L., and X.Z. S.L. provided the project infrastructure and supervised L.Y.'s study.

Method

First-principles band structure calculation: Electronic structures are calculated using density functional theory^{26,27} (DFT) based first-principles methods within the General Gradient Approximation (GGA)²⁸ implemented in the Vienna Ab initio simulation package (VASP)²⁹. A plane-wave expansion up to 400 eV is applied, and a Γ -centered $16 \times 16 \times 1$ Monkhorst-Pack³⁰ k-mesh is used for the Brillouin Zone sampling. The lattice constants used in the first-principles calculations are taken directly from the experimental data. The monolayer slab of BaNiS₂ are separated by a 17.8Å vacuum layer. We adopt the GGA+U method³¹ to account the on-site Coulomb interaction of localized Ni-3d orbitals. We follow the approach proposed by Neugebauer and Scheffler³² to apply a uniform electric field to monolayer BaNiS₂ slab in the calculations. This approach treats the artificial periodicity of the slab by adding a planar dipole sheet in the middle of the vacuum region. The strength of the dipole is calculated self-consistently such that the electrostatic field induced dipole is compensated for. For the calculations including the spin-orbit interaction, the spin quantization axis set to the default (0+, 0,1) (the notation 0+ implies an infinitesimal small positive number in x-direction) with zero atomic magnetic moments.

Table I. Examples of reported hidden physics in centrosymmetric crystals. Such hidden physics usually are forbidden to exist in high global crystal symmetry (GCS) but are allowed in individual local sectors with low local sector symmetry (LSS). Here, CS is short for centrosymmetric, non-CS for non-centrosymmetric, SHG for second harmonic oscillation, and AFE for antiferroelectricity. Non-CS polar point groups of LSS are explicitly C_1 , C_2 , C_3 , C_4 , C_6 , C_{1v} , C_{2v} , C_{3v} , C_{4v} , and C_{6v} . Non-CS non-polar point groups of LSS are D_2 , D_3 , D_4 , D_7 , S_4 , D_{2d} , C_{3h} , D_{3h} , T , T_d , and O .

| Polarization | Hidden functionality | Symmetry: LSS | Symmetry: GCS | Example |
|---------------------|-------------------------------|------------------------------|----------------------|---|
| Spin | Dresselhaus effect | Non-CS & Non-polar | CS | Si_2^6 , Ge_2^6 |
| | Rashba effect | Polar | CS | $BaNiS_2^{10,33}$, $LaOBiS_2^{11,34,35}$ |
| | Spin orbit torque in AFM | Non-CS | CS | $CuMnAs^{15}$, Mn_2Au^{16} |
| Orbital | Atomic orbital | Non-CS | CS | Ge_2 , $GaAs^{18}$ |
| Optical | Optical activity | Chiral | Non-chiral | $[Cu(H_2O)(bpy)_2]_2[HfF_6]_2 \cdot 3H_2O^{13}$ |
| Valley | Circular polarization | Non-CS | CS | Bilayer TMDs ¹⁴ |
| Electric | Antipiezoelectric | Non-CS & Non-polar exclude O | CS | BN^6 , $NaCaBi^6$ |
| | Antipiezo- & Antipyroelectric | Polar | CS | CdI_2^6 , $Bi_2Se_3^6$ |
| SHG | LA-SHG-2 | Non-polar | CS | Si_2^6 , $NaCaBi^6$ |
| | LA-SHG-2 & DF-SHG-2 | Polar | CS | MoS_2^6 , $Bi_2Se_3^6$ |

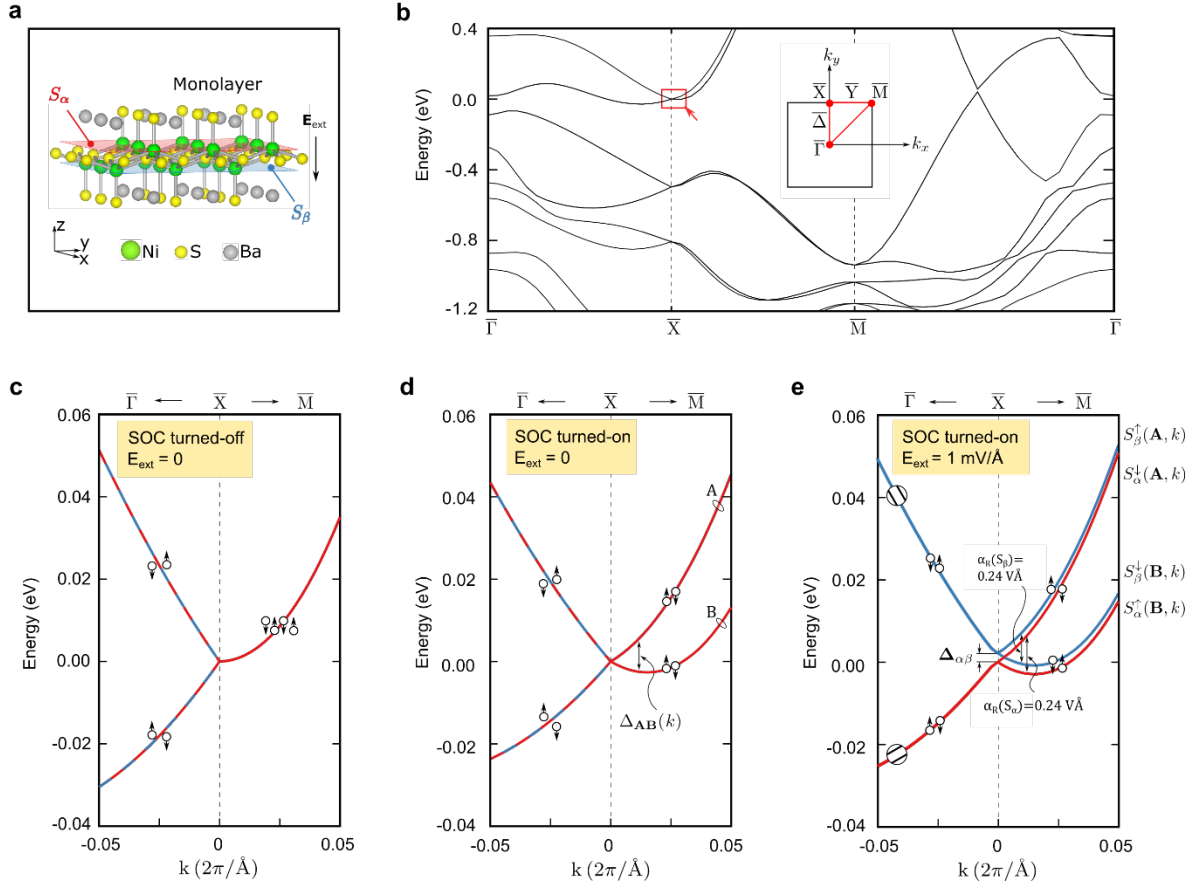


Figure 1 | The crystal structure and energy bands of the monolayer BaNiS₂. **a**, The crystal structure of a centrosymmetric monolayer of BaNiS₂ taken from the bulk with P4/nmm space group, showing its two inversion-partner sectors S_α and S_β . **b**, Energy band dispersion of the monolayer in an extended zone. The Rashba bands of interest are highlighted in red square. Insert shows schematically the 2D Brillouin zone of the monolayer. **c,d,e**, Zoom into the energy dispersion of the lowest four conduction bands near the X point along $\bar{X} - \bar{\Gamma}$ and $\bar{X} - \bar{M}$ directions when SOC is turned off (**c**) and turned on (**d,e**). However, in (**e**) a small electric field of 1 mV/Å is applied to the monolayer along the z-direction, as shown in **a**, to break the inversion symmetry. The inversion symmetry breaking electric field lifts degeneracy of both branches A and B into the S_α -Rashba-band and the S_β -Rashba-band, with an energy separation at the X point denote as $\Delta_{\alpha\beta}$. The band with its wavefunction segregated on the sector S_α is represented by red and on the on sector S_β by blue. Arrows are used to illustrate the spin orientation.

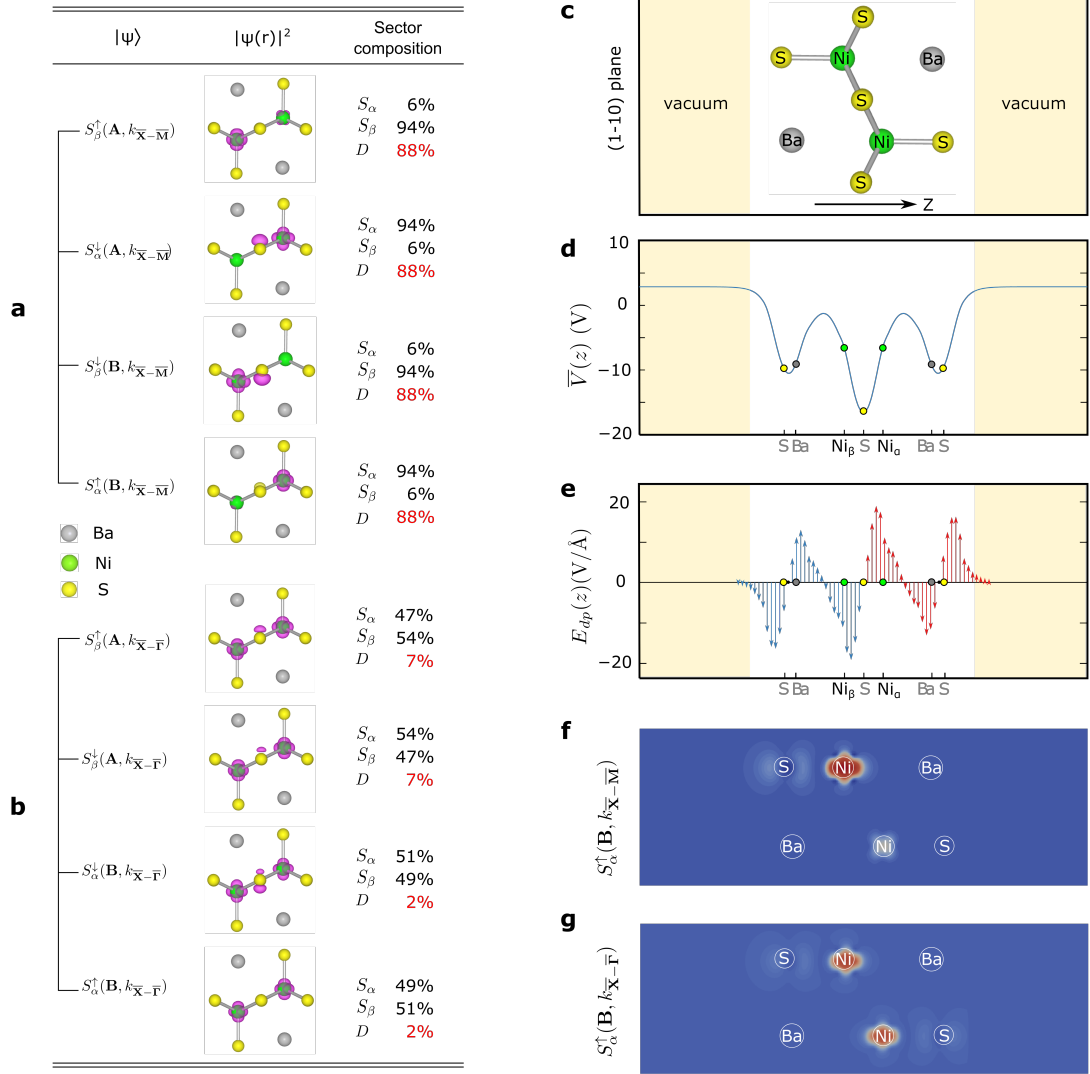


Figure 2 | Wavefunction segregation and local internal electric dipole fields in BaNiS₂ monolayer. **a, b**, Charge density of the lowest four conduction bands at $k_{\bar{\text{X}}-\bar{\Gamma}} = (0, 0.475, 0)(2\pi/a)$ and $k_{\bar{\text{X}}-\bar{\text{M}}} = (0.025, 0.5, 0)(2\pi/a)$, respectively. The isosurface of charge density is represented by purple as well as Ni, S, and Ba atoms represented by green, yellow, grey balls, respectively. The degree of wavefunction segregation (DWS) and the percentage of the charge density localized on the sectors S_α and S_β are also listed for each state. **c**, The crystal structure of the monolayer BaNiS₂ a view perpendicular to the (1-10) plane. **d**, Planar-averaged crystal potential of the monolayer BaNiS₂. **e**, The z-component of the internal local dipole fields $\mathbf{E}_{dp}(z) = (1/e) \partial \bar{V}(z) / \partial z$ along the z-direction. Red arrows indicate the dipole fields within the sector S_α and blue arrows for the dipole fields

within the sector S_β . **f, g**, Charge density of the $S_\alpha^\dagger(B, k_{\bar{X}-\bar{\Gamma}})$ and $S_\alpha^\dagger(B, k_{\bar{X}-\bar{M}})$ states of the monolayer BaNiS₂ in the absence of external fields.

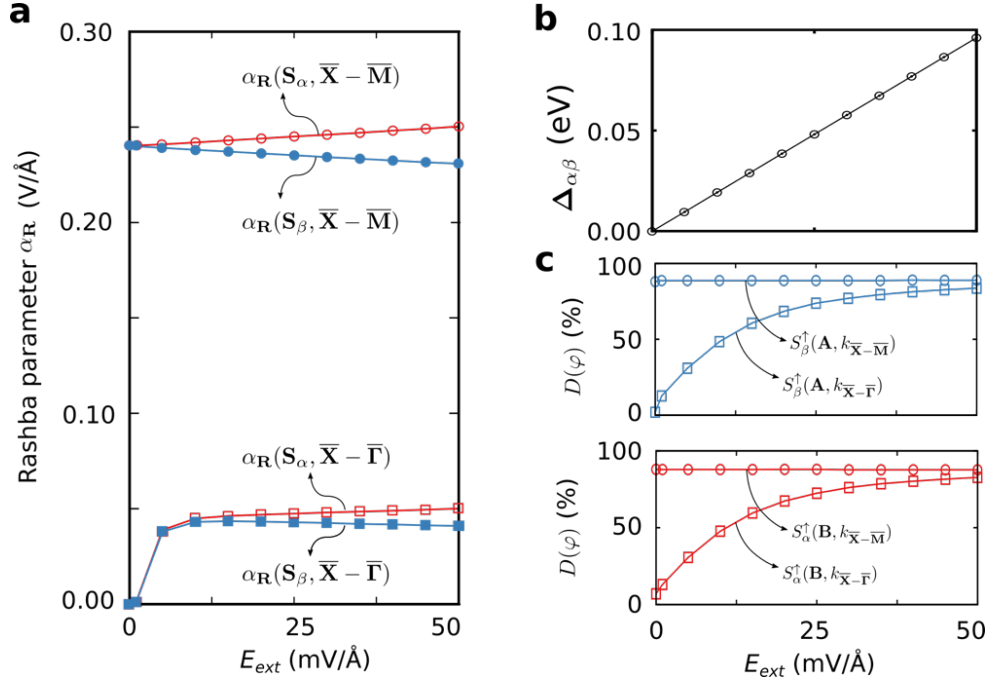


Figure 3 | The evolution of the Rashba parameters, and the corresponding degree of wavefunction segregation (DWS), as a function of the applied electric field in monolayer BaNiS₂. **a**, The Rashba parameters of the spin-splitting bands segregated on the sector S_α (empty squares or circles) and sector S_β (solid squares or circles), respectively, along $\bar{X} - \bar{\Gamma}$ (square) and $\bar{X} - \bar{M}$ (circle) directions as a function of applied electric field. **b**, Electric field induced energy separation ($\Delta_{\alpha\beta}$) between the S_α -Rashba-band and the S_β -Rashba-band at X point. **c**, Degree of wavefunction segregation (DWS) of branch A (upper) and branch B (lower) along $\bar{X} - \bar{\Gamma}$ and $\bar{X} - \bar{M}$ directions, respectively, as functions of the applied electric field. Note that the “Degree of Wavefunction Segregation” (DWS) of Eqs. (1)-(2) are used to describe qualitatively the trends as in Figs. 3c and 3d but the actual equation of α_R Eq. (3) with results displayed in Fig. 3a is a sum of dipole fields weighted by corresponding wavefunction amplitudes and thus does not display a simple linear correlation with the wavefunction segregation DWS.

References

- 1 Dresselhaus, G. Spin-Orbit Coupling Effects in Zinc Blende Structures. *Physical Review* **100**, 580-586, doi:10.1103/PhysRev.100.580 (1955).
- 2 Bychkov, Y. A. & Rashba, E. I. Oscillatory effects and the magnetic susceptibility of carriers in inversion layers. *Journal of physics C: Solid state physics* **17**, 6039 (1984).
- 3 Plum, E. *et al.* Metamaterials: optical activity without chirality. *Physical review letters* **102**, 113902 (2009).
- 4 Xiao, D., Yao, W. & Niu, Q. Valley-contrasting physics in graphene: magnetic moment and topological transport. *Physical review letters* **99**, 236809 (2007).
- 5 Mak, K. F., McGill, K. L., Park, J. & McEuen, P. L. The valley Hall effect in MoS₂ transistors. *Science* **344**, 1489-1492 (2014).
- 6 Zhang, X., Liu, Q., Luo, J.-W., Freeman, A. J. & Zunger, A. Hidden spin polarization in inversion-symmetric bulk crystals. *Nature Physics* **10**, 387-393, doi:10.1038/nphys2933 (2014).
- 7 Cheng, C., Sun, J.-T., Chen, X.-R. & Meng, S. Hidden spin polarization in the 1T-phase layered transition-metal dichalcogenides MX₂ (M = Zr, Hf; X = S, Se, Te). *Science Bulletin*, doi:<https://doi.org/10.1016/j.scib.2017.12.003>.
- 8 Razzoli, E. *et al.* Selective Probing of Hidden Spin-Polarized States in Inversion-Symmetric Bulk MoS₂. *Physical review letters* **118**, 086402, doi:10.1103/PhysRevLett.118.086402 (2017).
- 9 Riley, J. M. *et al.* Direct observation of spin-polarized bulk bands in an inversion-symmetric semiconductor. *Nature Physics* **10**, 835-839, doi:10.1038/nphys3105 (2014).
- 10 Santos-Cottin, D. *et al.* Rashba coupling amplification by a staggered crystal field. *Nature communications* **7** (2016).
- 11 Wu, S.-L. *et al.* Direct evidence of hidden local spin polarization in a centrosymmetric superconductor LaO_{0.55}F_{0.45}BiS₂. *Nature communications* **8**, 1919, doi:10.1038/s41467-017-02058-2 (2017).
- 12 Yao, W. *et al.* Direct observation of spin-layer locking by local Rashba effect in monolayer semiconducting PtSe₂ film. *Nature communications* **8**, 14216, doi:10.1038/ncomms14216 (2017).
- 13 Gautier, R., Klingsporn, J. M., Van Duyne, R. P. & Poeppelmeier, K. R. Optical activity from racemates. *Nature materials* **15**, 591-592 (2016).
- 14 Liu, Q., Zhang, X. & Zunger, A. Intrinsic circular polarization in centrosymmetric stacks of transition-metal dichalcogenide compounds. *Physical review letters* **114**, 087402 (2015).
- 15 Wadley, P. *et al.* Electrical switching of an antiferromagnet. *Science* **351**, 587-590, doi:10.1126/science.aab1031 (2016).
- 16 Železný, J. *et al.* Relativistic Néel-Order Fields Induced by Electrical Current in Antiferromagnets. *Physical review letters* **113**, 157201, doi:10.1103/PhysRevLett.113.157201 (2014).
- 17 Liu, C.-X. Unconventional Superconductivity in Bilayer Transition Metal Dichalcogenides. *Physical review letters* **118**, 087001, doi:10.1103/PhysRevLett.118.087001 (2017).
- 18 Ryoo, J. H. & Park, C.-H. Hidden orbital polarization in diamond, silicon, germanium, gallium arsenide and layered materials. *NPG Asia Materials* **9**, e382, doi:10.1038/am.2017.67 (2017).
- 19 Li, P. & Appelbaum, I. Illuminating" spin-polarized" Bloch wave-function projection from degenerate bands in decomposable centrosymmetric lattices. *Physical Review B* **97**,

- 125434 (2018).
- 20 Luo, J.-W., Li, S.-S. & Zunger, A. Rapid Transition of the Hole Rashba Effect from Strong Field Dependence to Saturation in Semiconductor Nanowires. *Physical review letters* **119**, 126401 (2017).
 - 21 Grey, I. & Steinfink, H. Crystal structure and properties of barium nickel sulfide, a square-pyramidal nickel (II) compound. *Journal of the American Chemical Society* **92**, 5093-5095 (1970).
 - 22 Santos-Cottin, D. *et al.* Anomalous metallic state in quasi-two-dimensional BaNiS₂. *Physical Review B* **93**, 125120 (2016).
 - 23 Winkler, R. Spin-orbit coupling effects in two-dimensional electron and hole systems. *Springer Tracts in Modern Physics* **191**, 153-156 (2003).
 - 24 Condon, E. U. Notes on the Stark Effect. *Physical Review* **43**, 648-654, doi:10.1103/PhysRev.43.648 (1933).
 - 25 Tsai, H. *et al.* Clear variation of spin splitting by changing electron distribution at non-magnetic metal/Bi2O3 interfaces. *Scientific Reports* **8**, 5564, doi:10.1038/s41598-018-23787-4 (2018).
 - 26 Sham, L. J. & Schlüter, M. Density-Functional Theory of the Energy Gap. *Physical review letters* **51**, 1888-1891 (1983).
 - 27 Gross, E. K. & Dreizler, R. M. *Density functional theory*. Vol. 337 (Springer Science & Business Media, 2013).
 - 28 Perdew, J. P., Burke, K. & Ernzerhof, M. Generalized Gradient Approximation Made Simple. *Physical review letters* **77**, 3865-3868 (1996).
 - 29 Kresse, G. & Furthmüller, J. Efficiency of ab-initio total energy calculations for metals and semiconductors using a plane-wave basis set. *Computational materials science* **6**, 15-50 (1996).
 - 30 Monkhorst, H. J. & Pack, J. D. Special points for Brillouin-zone integrations. *Physical Review B* **13**, 5188-5192, doi:10.1103/PhysRevB.13.5188 (1976).
 - 31 Liechtenstein, A., Anisimov, V. & Zaanen, J. Density-functional theory and strong interactions: Orbital ordering in Mott-Hubbard insulators. *Physical Review B* **52**, R5467 (1995).
 - 32 Neugebauer, J. & Scheffler, M. Adsorbate-substrate and adsorbate-adsorbate interactions of Na and K adlayers on Al(111). *Physical Review B* **46**, 16067-16080, doi:10.1103/PhysRevB.46.16067 (1992).
 - 33 Sławińska, J., Narayan, A. & Picozzi, S. Hidden spin polarization in nonmagnetic centrosymmetric BaNiS₂ crystal: Signatures from first principles. *Physical Review B* **94**, 241114 (2016).
 - 34 Liu, Q., Guo, Y. & Freeman, A. J. Tunable Rashba effect in two-dimensional LaOBiS₂ films: ultrathin candidates for spin field effect transistors. *Nano letters* **13**, 5264-5270, doi:10.1021/nl4027346 (2013).
 - 35 Liu, Q. *et al.* Search and design of nonmagnetic centrosymmetric layered crystals with large local spin polarization. *Physical Review B* **91**, doi:10.1103/PhysRevB.91.235204 (2015).